Cylindrical wave approach to observe the scattering of surface plasmon-polariton waves from a cylinder

---

By

Abdul Rehman

Department of Electronics

Quaid-i-Azam university

Islamabad, Pakistan

2019

Cylindrical wave approach to observe the scattering of surface plasmon-polariton waves from a cylinder

By

Abdul Rehman

Submitted in partial fulfillment of the
requirement for the degree of
Master of Philosophy
at
Quaid-i-Azam University
Islamabad, Pakistan
July 2019

QUAID-I-AZAM UNIVERSITY
DEPARTMENT OF
ELECTRONICS

The undersigned hereby certify that they have read and recommend to the Faculty of Graduate Studies for acceptance a thesis entitled "**Cylindrical wave approach to observe the scattering of surface plasmon-polariton waves from a cylinder**" by **Abdul Rehman** in partial fulfillment of the requirements for the degree of **Master of Philosophy**.

Dated: July 2019

Research Supervisor: _____

Chaiman: _____

QUAID-I-AZAM UNIVERSITY

Date: **July 2019**

Author: **Abdul Rehman**

Title: **Cylindrical wave approach to observe the scattering of surface plasmon-polariton waves from a cylinder**

Department: **Electronics**

Degree: **M.Phil.** Year: **2019**

Signature of Author

To "Almighty creator"

Who put my soul in Human shell

To "Prophet Muhammad(PBUH)"

the perfect man to follow

To "my parents"

for their limitless sacrifices

and

To "Allians", Which I speculate they exist.

Table of Contents

List of Figures

Acknowledgements

In the Name of Allah, the Most Merciful, the Most Compassionate all praise be to Allah, the Lord of the worlds; and prayers and peace be upon Mohammed His servant and messenger. First and foremost, I must acknowledge my limitless thanks to Allah, the Ever-Magnificent; the Ever-Thankful, for His help and bless.I am totally sure that this work would have never become truth, without His guidance.

I am grateful to some people, who worked hard with me from the beginning till the completion of the present research particularly my supervisor Dr. Arshad Fiaz, who has been always generous during all phases of the research, and I highly appreciate the guidance by Dr. M. Faryyad from LUMS University.

I owe profound gratitude to my Father, Mother and Uncle for their constant encouragement, limitless giving and great sacrifice, helped me accomplish my degree.I also would like to express my wholehearted thanks to my family for their generous support they provided me. I am very appreciative to my colleagues and Lab Mates, who participated in this study. I am also grateful to my friends at my hometown, Without their them, this study would be boring and colorless. Last but not least, deepest thanks go to all people who took part in making this thesis real.

Abdul Rehman

july, 2019

Abstract

Surface waves are the solutions of Maxwell's equations in the frequency domain at the flat interface of two different materials. Poynting vector averaged over time has a significant component parallel to the interface decays at sufficiently large distances normal to the interface. If one of the partnering materials is a metal and the other a dielectric, the surface waves are called surface plasmon-polariton (SPP) waves.

Surface plasmon-polariton (SPP) waves are the most extensively studied waves among various types of surface waves because they are easy to excite and have been used in many optical applications particularly for plasmonic communication, sensing, and harvesting solar energy. In all of these applications, especially on-chip plasmonic communication, scattering can be an important issue to contend with. Therefore, the objective of this paper is to theoretically inspect the scattering pattern of SPP waves from a perfect electric conductor (PEC) cylindrical scatterer. The cylindrical wave approach is used to solve the scattering problem by a cylindrical object placed below a metallic layer. The scattering is investigated thoroughly by changing the size of the scatterer and its distance from the interface along which the SPP wave is excited. As size of the scatterer increases, the scattering increases significantly. On the other hand, when the distance of the scatterer from the interface is increased, the scattered field becomes small. Two-dimensional field maps are produced for the incidence angle at which SPP is excited. Numerical results are also presented for other incidence angles to make a comparison. Furthermore, the forward and backward far-fields are significantly enhanced if the SPP wave is scattered in comparison to when SPP wave is not present.

Chapter 1

Introduction

The goal of this research conducted as part of this thesis has been to excite and theoretically study the scattering of surface plasmon-polariton (SPP) waves at a particular frequency from an object placed beneath a metallic partnering material in a dielectric medium. Scattering of the SPP waves by different sizes of objects placed at different distances under the interface along which the SPP waves were enthusiastically studied, especially for this thesis. SPP waves find applications in optical sensing, solar photovoltaics, and on-chip optical communications and computing [1]-[2]. Plasmonic communication is the emerging future for ultra-fast communication. The development of new optical devices used in communication is getting better and researchers are finding keen interest in this field. This progress is making possible the plasmonic nanocircuits leading to demonstrate plasmonic data generation, transport and detection [3]-[7]. The applications of SPP waves in on-chip communications can suffer from the scattering losses during signal propagation leading to the loss of power and distortion of shape of the pulses. Therefore, it is very important to understand the scattering mechanisms and characteristics for ubiquitous applications of plasmonic communication.Therefore, we set out to investigate the scattering of the SPP waves from a simple canonical object, that is, a circular cylinder made of a good conductor.

Spectral domain method is used for investigating scattering from objects located under a dielectric-metal interface. The propagating fields are analytically represented

by the CWA (Cylinder Wave Approach) technique. Scattered fields are expressed by the spectra of plane waves. By interacting with a layer layout, scattered fields at the boundary of the layer are reflected infinitely. By using appropriate coefficients for reflection and transmission within the spectra, the interaction is solved. Two sets of multiple reflections are generalized, upward fields from the scatterer and downward propagation reaching to the scatterers through the layer. Consequently, for numerical implementation this analytic theory compact and efficient. The numerical outcome is evaluated accurately and validated by comparison with the results reported in the literature. The scattered field may be evaluated at any point, both in the far and near region.

1.1 Surface plasmon-polaritons

Surface plasmon-polaritons (SPP) are electromagnetic waves of an infrared or visible frequency that propagates along with metals - dielectric/air interface. 'Surface Plasmon' describes a charge motion in metal and 'Polaritons' explains electromagnetic waves in dielectric/air.

Among various electromagnetic surface waves, the SPP wave has the longest theoretical and historical development [8]-[10]. Zenneck [11] proposed, a century before, that in the microwave region an electromagnetic wave might propagate along with the air-ground interface of planes. Sommerfeld [12] provided a rigorous mathematical analysis of what is called the Zenneck wave [13]-[26]. The basic concept reappeared about 60 years ago [15] in the form of SPP waves driven by guided boundary of two, dielectric homogenous and isotropic materials. The real parts of the two homogeneous, isotropic, and dielectric have opposite signs [16]-[17] of relative permittivity. In general, the material of the relation with real negative permittivity is a metal [18], but other materials may also be suitable [19]-[20]. The theory has evolved to understand the interfaces between metal and various complex dielectric materials. In the study of surface waves, the homogeneous and anisotropic dielectric materials [21]-[28] have been considered for some time. Surface waves, which are directed through a

metallic material and a periodically nonhomogeneous dielectric interface, have noteworthy characteristics [29]. The non-homogeneous dielectric materials studied, take account of continuously varying materials like cholestatic liquid crystals [29]-[32] and layered structures [33]-[36].

Various dielectric materials will be polarized specifically when the interaction of the electromagnetic field occurs, thus providing a technique commonly used for the detection of chemical and biochemical substances [37]-[38]. In addition, for high throughput analysis of bio-molecular interactions for proteomics, drug discovery, and trail illumination [39]-[40] SPP imaging/sensing systems are used. Even imaging techniques based on SPP will be useful for lithography [16]-[42]. SPP based detection systems are working effectively to detect bio-affinity interactions with DNA, carbohydrates, proteins, and peptides [41]. Lastly, since SPP waves may be excited in terahertz/optical regions, they are useful for ultra speed information communication chips [43]. Although, at frequencies, more than a few tens of GHz usual cables are very weak and ohmic losses to plasmonic transmission are minimum [17], which allows long-distance communication [44].

The solution to the canonical boundary valued problem [16]-[17] and [38] at specific frequency shows that if the associated material is dielectric, isotropic, and homogeneous, a single SPP wave can propagate through an interface. The same result is valid for anisotropic material [23]-[45]. Although, if the associated material is dielectric, periodically anisotropic and homogeneous normal to the interface, the canonical problem [29] indicates that multiple SPP waves with different attenuation rates, several phase velocities, and field distributions can be propagated by the interface at the same frequency [30]. Experimental confirmation of this theoretical prediction has been found [46]-[47]. In addition, some researchers [48] -[50] have revealed that experimentally and theoretically s-polarized surface waves may be directed at the interface of multilayered dielectric material and metal.

1.1.1 Practical configurations to excite Surface waves

To excite the SPP wave, a photon should have momentum and frequency the same as SPP. Although, at a specific frequency, a photon from free space has less momentum than SPP wave as a result of the difference in dispersion relations. This incompatibility of the momentum is one cause why a free space photon may not couple directly to SPP. Therefore, for a similar basis on a smooth metal surface, an SPP cannot emanate energy like a free space photon into the dielectric. This inaptness is similar to the lack of transmission that occurs for the duration of total internal reflection.

The incompatibility between SPP and plane waves prevents SPP waves from being excited in the bulk associated dielectric material as a result of direct coupling. Therefore, four configurations are in practice to stimulate SPP waves, a couple of prism linked configurations, grating coupled configurations, and waveguide coupled. Even though these configurations are correspondent to one another to excite the SPP wave, but each one is appropriate for different applications. In addition, when cautious analysis of experimental or calculated data is required from these configurations, the remedy should be made to canonical boundary value problem for solution.

1.1.2 Prism Coupled Configuration

The most common configuration to excite the SPP wave is coupled to the prism using the attenuated total reflection (ATR). There are two configurations to implement the coupling of the prism: Turbadar-Kretschmann-Raether (TKR) and Turbadar-Otto (TO) [37]. In the TKR configuration, as shown in figure 1.1, a prism having a high refractive index is connected with a thin dielectric layer and a metal. An oil of refraction index equal to that of the prism is used between the prism and the metal to eliminate air bubbles when the light propagates in the prism is made incident on the metal film, part of which is reflected towards the prism and a part is refracted in the metal. The wave refracting into metal decreases exponentially, in the perpendicular direction to the prism/metal interface. If the metallic film of the interface is thin enough, the wave penetrates from the metallic material and is coupled to the SPP

in the metal/dielectric limiting interface. At a particular incidence angle to prism and metal interface, electromagnetic boundary conditions are satisfied to instigate the SPP wave at metal and dielectric interface.

If the dielectric and the metal films are interchanged in the TKR configuration, the new configuration is called the TO configuration. In this configuration (see Figure 1.1), the incident field on the prism and the dielectric interface at greater than the critical angle an evanescent wave in the partnering dielectric materials is produced. If the dielectric film is thin enough, the phase velocity of the evanescent wave propagating parallel to the interface and the SPP wave that propagates along the dielectric-metallic interface is identical. A TKR configuration may be used only for the excitation of SPP waves while TO configuration can also be used to launch Tamm waves or Dyakonov waves besides SPP, if the metal film is replaced respectively by an isotropic or anisotropic material but periodically non- homogeneous dielectric.

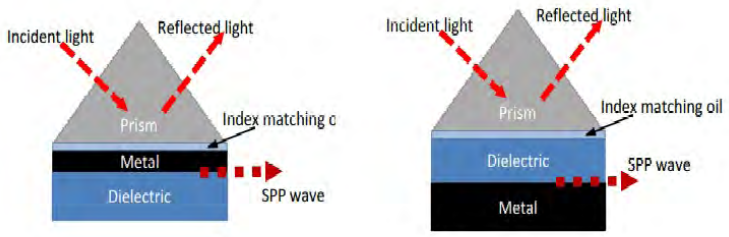

Figure 1.1: TKR configuration and TO configuration, respectively

The prism-coupled configuration is mainly useful for stimulating an SPP wave with the desired polarization state and is easy to put into practice. Yet, care must be taken to distinguish between the SPP waves driven along with the metal-dielectric interface and the waveguide modes propagating in the bulk of the associated dielectric material of finite thickness.

1.1.3 Grating-Coupled Configuration

A substitute to the TKR configuration is the grating-coupled configuration, as shown in Figure 1.2. This configuration is generally used to excite SPP waves; however, it can also be used to excite the Tamm and Dyakonov-Tamm waves. To excite the SPP waves in this configuration, it is necessary to illuminate the periodic corrugations of a metal embossed network coated with the dielectric partner material. The fields of the two partnering materials must be represented by linear overlaps of Floquet harmonics. If the wave vector component of a harmonic Floquet in the grid plane is identical to that of the SPP wave, the Floquet harmonics can be coupled with the SPP wave. The grating-coupling also allows the inverse process of the coupling of non-radiating SPP with light [52]-[53]. This is a significant benefit over TKR and allows much better integration with SPP-based chemical sensors [54] into integrated optical circuits [55].

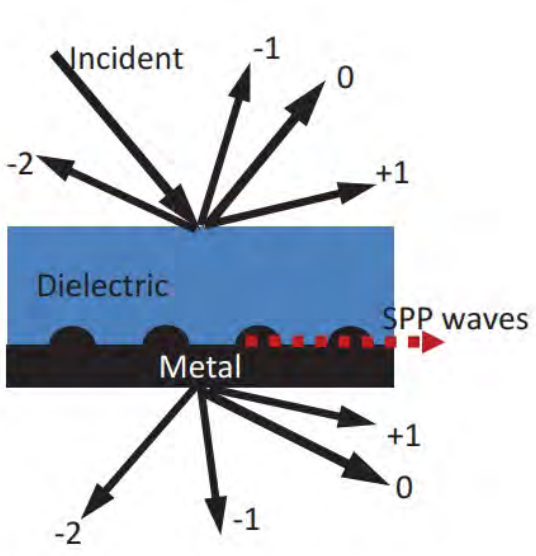

Figure 1.2: grating-coupled configuration

This configuration is mainly useful if it is desired to excite multiple SPP waves at the same time using a finite light source or a quasi-periodic surface-relief grating.

1.1.4 Waveguide-Coupled Configuration

A less common technique for exciting SPP waves is to use an optical dielectric waveguide. Typically, a dielectric waveguide is incorporated with a metal-dielectric interface, as shown in Figure 1.3. When a waveguide mode propagating in the dielectric waveguide has the same phase velocity as metal-dielectric interface guided SPP wave, the electromagnetic energy of waveguide mode in dielectric waveguide couples with the SPP driven by the metallic-dielectric interface.

This configuration has the advantage of exciting SPP waves directly in the metal-dielectric interface. We are going to use this configuration to excite the SPP wave in dielectric partnering material in which the cylinder is buried to observe the scattering of the SPP wave.

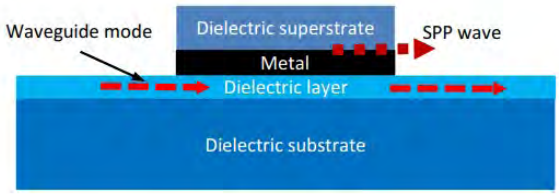

Figure 1.3: waveguide-coupled configuration

1.2 Two Dimensional Scattering Problem

The problem of electromagnetic scattering by buried targets has already been addressed by many authors, both by theoretically [56]-[57] and numerically [58]-[59]. Researchers are constantly exploiting this problem, through remote sensing to observe the earth's internal structure, mines finding, detecting tunnels and conduits, to the communication in the course of the earth and to biomedical imaging. For

solving 2-D scattering problems different techniques and procedures have been used. Howard [56] used the mode adjustment technique for solving a two-dimensional integral equation of the scattered field. To get simple numerical results, Ogunade [60] has proceeded further on previous work [61]. Mahmoud et al. [62] worked on a multipole expansion of the scattered field. The explanation for the evaluation of different forms of the kernel is solved by Butler et al. [63]. Hongo et al. [64] dealt with the scattering of plane waves by 2-D cylindrical objects placed in a dielectric semi-infinite medium according to Kobayashi potential method [65]. A revised and corrected version of [64] has been reported in [66]. for the asymptotic solutions obtained by the saddle-point method, applied to the much larger distance between the obstacle of different sizes and the interface than the wavelength. In [67] the electromagnetic scattering by PEC objects of random shape implanted in a laminate media was developed theoretically.

A high frequency beam/ray tracing technique is used in [68] to characterize the interior of a building. Using CWA in [69], scattering from perfectly conducting cylinders buried beneath a dielectric slab/layer is determined in the frequency domain. The rules of the CWA implemented in approach [69] were followed in [71]. In [69], an iterative approach is used to solve the reflection and transmission of the scattered fields. Appropriate reflection and transmission coefficients are used as basis functions within the spectral integral functions of the scattered fields to evaluate multiple reflections within the slab/layer. As part of the approach used in [69] and [70], newly developed functions in cylindrical waveform were presented in [71] to effectively handle two flat boundaries. The convergence of this newly developed approach [71] with the previous theory which deals with multiple reflections in [69] is satisfied. Therefore, this Non-iterative approach is used in this dissertation.

1.2.1 Cylindrical Wave Approach

CWA is an efficient procedure in the spectral domain to obtain a meticulous solution of 2-D scattering problems. The CWA solves in the spectral domain. In this technique, the field scattered by buried objects is expressed by the superposition of

cylindrical waves. Work is done on the plane wave spectra taking into account multiple interactions of these waves with the flat air/soil interface and between the different layers present. The phenomena of multiple reflection, transmission, and scattering are taken into account. This technique is applicable for arbitrary values of the permittivity, size, and location of the targets, and for arbitrary values of the permittivity of the host media, which may be lossy or lossless. As the technique is implemented in the spectral domain, dispersive mediums can be modeled easily. Targets of general shape can be simulated with outstanding results, by approximating them with a suitable set of small circular cylinders. This method can also be used to study the propagation of incident pulsed-wave having a general shape in the time-domain. Also, a version of the CWA extended to understand the roughness in the air-soil interface. In general, CWA allows the excellent modeling of the environment, it is exploiting and improving overall performance in the field of GPR, which makes it worth being exploring and developing. We used this technique in our study for this thesis after carefully observing the results produced by CWA, which are consistent and well-matched with the literature.

1.3 Objectives of the Thesis

The objectives of the research carried out for this dissertation were to:

- excite the SPP wave in the partnering dielectric materials;
- to calculate the scattered SPP field using CWA approach;
- explicate the scattering of SPP waves by varing the size and location of the scattere for experimental research;
- investigate scattering pattern in the presence of SPP waves.

Chapter 2

Scattering from a cylinder placed under a dielectric layer

In this chapter, we formulated the scattering solution from a perfectly conducting cylinder placed under a dielectric/metllic layer. The solution is developed using the CWA. In CWA we used the cylindrical function as basis function for the computation of scattered fields.

2.1 Analytical formulation

Let us consider the schematic geometry in Fig. 2.1. The configuration used to excite the SPP wave is Turbadar–Kretschmann–Raether (TKR) configuration [73]-[75]. Medium 1 in the geometry is a dielectric material with permittivity $\epsilon_1 = \epsilon_0\epsilon_{r1}$ which is essentially a high-refractive index medium working as a prism for the excitation of SPP waves. Medium 2 is a metallic layer with permittivity $\epsilon_2 = \epsilon_0\epsilon_{r2}$ and medium 3 hosting the PEC cylinder has the permittivity $\epsilon_3 = \epsilon_0$. All media are non-magmatic, homogenous, linear and isotropic. A temporal dependency $exp(-i\omega t)$ is taken implicitly where ω represents the angular frequency.

The primary reference frame (PRF) (O, ξ, ζ) is represented by the normalized coordinates $\xi = k_0 x$ and $\zeta = k_0 z$, whereas $k_0 = \omega/c$ is the wave number of free space. The secondary reference frame (SRF) is centered at the center of the cylinder

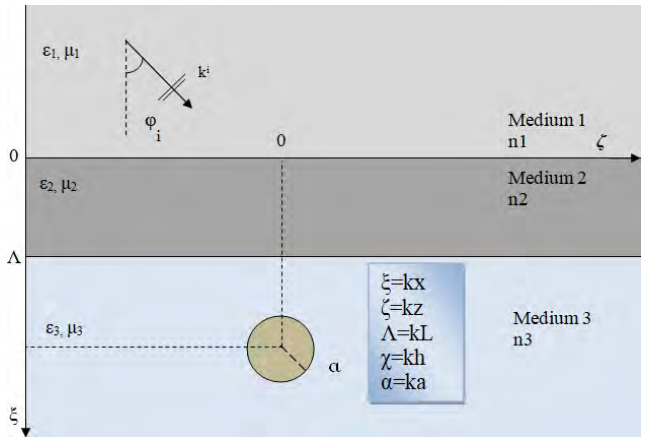

Figure 2.1: A plane wave propagating in medium 1 is incident on the interface between medium 1 and medium 2 having refractive index n_1 and n_2, respectively. A PEC cylinder is placed at distance χ below the second interface at $\xi = \Lambda$ in medium 3 with permittivity n_3.

as (O, ξ_1, ζ_1) and (O, ρ, θ) in the cartesian and the polar coordinates systems, respectively, where $\xi_1 = \xi - \chi$, $\zeta_1 = \zeta - \eta$ and $\rho = k_0 r$. The PEC cylinder is centered at (χ, η) with normalized radius is $\alpha = k_0 a$.

A monochromatic incident plane wave of amplitude ψ_0 propagating in the medium 1 is considered as a source. The incident field can be written as:

$$\Psi_i(\xi, \zeta) = \psi_0 e^{i(n_1 n_\perp^{\mathrm{i}} \xi + n_1 n_\parallel^{\mathrm{i}} \zeta)}, \qquad \xi < 0, \quad (2.1.1)$$

where n_1 is the refractive index of the dielectric half-space, $n_\parallel^{\mathrm{i}}$ is parallel and $n_\perp^{\mathrm{i}}$ is orthogonal components of incident wave vector. They are related to the incidence angle φ_i as:

$$n_\parallel^{\mathrm{i}} = \sin(\varphi_i)\,, \qquad n_\perp^{\mathrm{i}} = \sqrt{1 - (n_\parallel^{\mathrm{i}})^2}\,.$$

In the following, we present a unified formulation for the TM and the TE polarization states. Since they are isomorphic, the following identification can be made for the two linear polarization states:

$$\mathrm{TM - Polarization :} \qquad \Psi(\xi, \zeta) = E_y(\xi, \zeta)$$
$$\mathrm{TE - Polarization :} \qquad \Psi(\xi, \zeta) = H_y(\xi, \zeta)$$

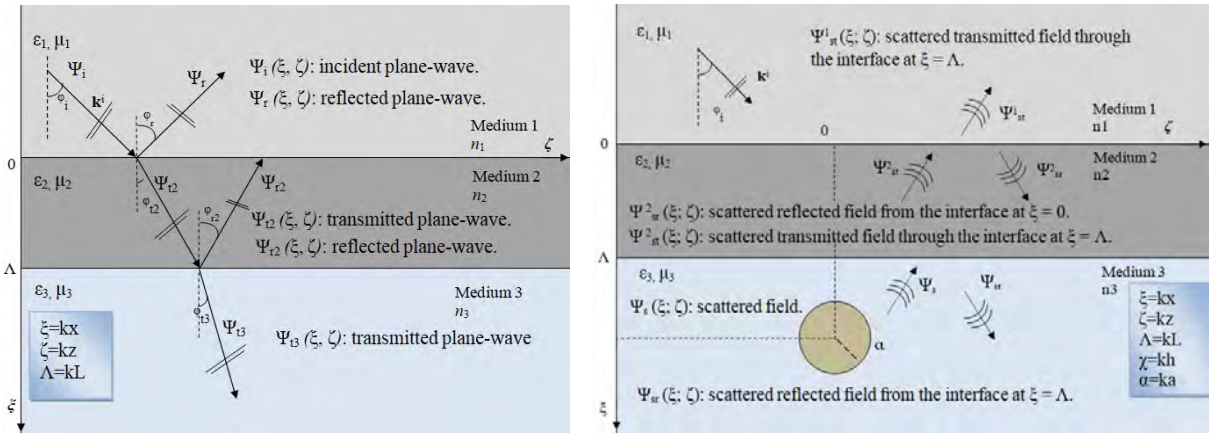

(a) Transmitted and reflected plane-wave contributions when the PEC cylinder is not present.

(b) Scattered, scattered-transmitted and scattered-reflected fields due to the presence of the PEC cylinder.

Figure 2.2: Schematic representation of all propagating-field contributions: (a) without cylinder and (b) with cylinder.

The function $\Psi(\xi,\zeta)$ is used to represent the superposition of multiple field contributions in each medium triggered by the interaction of the incident field with both the scatterer and the interfaces. This scattering problem has two scenarios. First, we evaluated the field contributions without cylinder, as shown in Fig. 2.2(a). These fields are propagating in layered background and can be written by [71], as:

$$\Psi_r(\xi,\zeta) = \psi_0 \Gamma_{12}(n_{\parallel}^{\mathrm{i}})\; e^{in_1(-n_{\perp}^{\mathrm{i}}\xi + n_{\parallel}^{\mathrm{i}}\zeta)}, \qquad \xi < 0, \quad (2.1.2)$$

$$\Psi_{\mathrm{t2}}(\xi,\zeta) = \psi_0 T_{12}(n_{\parallel}^{\mathrm{i}})\; e^{in_2[n_{\perp}^{\mathrm{t2}}(\xi-\Lambda) + n_{\parallel}^{\mathrm{t2}}\zeta]}, \qquad 0 < \xi < \Lambda, \quad (2.1.3)$$

$$\Psi_{\mathrm{r2}}(\xi_{\mathrm{p}},\zeta_{\mathrm{s}}) = \psi_0 T_{12}(n_{\parallel}^{\mathrm{i}})\Gamma_{23}(n_{\parallel}^{\mathrm{i}})\; e^{in_2\left[-n_{\perp}^{\mathrm{t2}}(\xi-\Lambda) + n_{\parallel}^{\mathrm{t2}}\zeta\right]}, \qquad 0 < \xi < \Lambda, \quad (2.1.4)$$

$$\Psi_{\mathrm{t3}}(\xi,\zeta) = \psi_0 T_{12}(n_{\parallel}^{\mathrm{i}})T_{23}(n_{\parallel}^{\mathrm{i}})\; RW_{\mathrm{m}} e^{in_3\left[-n_{\perp}^{\mathrm{t3}}(\xi-\Lambda) + n_{\parallel}^{\mathrm{t3}}\zeta\right]}, \qquad \xi > \Lambda, \quad (2.1.5)$$

where Γ_{12}, Γ_{23} and T_{12}, T_{23} are reflection and transmission coefficients [**?**], respectively, whereas $n_{\perp}^{\mathrm{t2}}, n_{\perp}^{\mathrm{t3}}$ and $n_{\parallel}^{\mathrm{t2}}, n_{\parallel}^{\mathrm{t3}}$ are orthogonal and parallel components, respectively, which can be derived from Snell's law [71].

Let us now discuss the second scenario when PEC cylinder is present in medium 3. The incident plane wave after transmission through metallic layer reaches medium 3 and interacts with the cylinder. A scattered field is excited and expressed as the superposition of cylindrical function.

$$CW_\ell(\xi,\zeta) = \mathrm{H}_\ell^{(1)}(\rho)\mathrm{e}^{\mathrm{i}\ell\theta}\,, \quad \ell \in \{0, \pm1, \pm2, ...\}$$

where $H_\ell^{(1)}$ represents the Hankel function of first-kind of integer order ℓ.

The field scattered by cylinder can be represented with unknown coefficient c_m in terms of cylindrical wave function CW_ℓ as [71]:

$$\Psi_\mathrm{s}(\xi,\zeta) = \psi_0 \sum_{m=-\infty}^{+\infty} c_\mathrm{m} CW_\mathrm{m}(n_3\xi, n_3\zeta)\,, \qquad \xi > \Lambda \quad (2.1.6)$$

The fields shown in Fig. 2.2(b) except Ψ_s are excited as a result of interactions of Ψ_s with the planar interfaces. Their expressions are represented by cylindrical wave function CW_m in terms of Fourier spectrum of all plane wave reflections and transmissions from interfaces with unknown coefficient c_m as in equation (6). Therefore, from the similar approach used in [71], the cylindrical function CW_m in terms of Fourier spectrum can be written as:

$$CW_\mathrm{m}(\xi, n_\parallel) = \frac{1}{2\pi} \int_{-\infty}^{+\infty} F_\mathrm{m}(\xi, n_\parallel) e^{in_\parallel\zeta} dn_\parallel, \qquad (2.1.7)$$

where the Fourier spectrum can be written as:

$$F_\mathrm{m}(\xi, n_\parallel) = \frac{2\, e^{i|\xi|\sqrt{1-n_\parallel^2}}}{\sqrt{1-n_\parallel^2}} \begin{cases} e^{-i\mathrm{m}\cos^{-1} n_\parallel}, & \xi \le 0\,, \\ e^{i\mathrm{m}\cos^{-1} n_\parallel}, & \xi \ge \Lambda\,, \end{cases} \qquad (2.1.8)$$

The scattered-reflected field Ψ_sr, reflected from the interface at $\xi = \Lambda$ can be written as:

$$\Psi_\mathrm{sr}(\xi,\zeta) = \psi_0 \sum_{\mathrm{m}=-\infty}^{\infty} c_\mathrm{m} RW_\mathrm{m}[-n_3(\xi + \chi_\mathrm{p} - 2\Lambda), n_3(\zeta - \eta)], \qquad \xi > \Lambda, \quad (2.1.9)$$

where

$$RW_{\mathrm{m}}(\xi,\zeta)=\frac{1}{2\pi}\int_{-\infty}^{\infty}\Gamma_{32}(n_{\parallel})F_{\mathrm{m}}(\xi,n_{\parallel})e^{in_{\parallel}\zeta}dn_{\parallel}\,, \tag{2.1.10}$$

Similarly, the scattered-transmitted field Ψ^2_{st} can be written as:

$$\Psi^2_{\mathrm{st}}(\xi,\zeta)=\psi_0\sum_{\mathrm{m}=-\infty}^{\infty}c_{\mathrm{m}}TW^2_{\mathrm{m}}(\xi,\zeta,\chi) \qquad 0<\xi<\Lambda, \tag{2.1.11}$$

where the basis function can be written as:

$$TW^2_{\mathrm{m}}(\xi,\zeta;\chi)=\frac{1}{2\pi}\int_{-\infty}^{\infty}T_{32}(n_{\parallel})F_{\mathrm{m}}\left[-n_3(\chi-\Lambda),n_{\parallel})\right]\,e^{in_2\sqrt{1-(n_3n_{\parallel}/n_2)^2}(\xi-\Lambda)}e^{in_3n_{\parallel}(\zeta-\eta)}dn_{\parallel}\,, \tag{2.1.12}$$

The scattered-reflected field Ψ^2_{sr} can be written as:

$$\Psi^2_{\mathrm{sr}}(\xi,\zeta)=\psi_0\sum_{\mathrm{m}=-\infty}^{\infty}c_{\mathrm{m}}RW^2_{\mathrm{m}}(\xi,\zeta;\chi,\Lambda), \qquad 0<\xi<\Lambda, \tag{2.1.13}$$

where the basis functions are:

$$RW^2_{\mathrm{m}}(\xi,\zeta;\chi,\Lambda)=\frac{1}{2\pi}\int_{-\infty}^{\infty}T_{32}(n_{\parallel})\Gamma_{21}(n_{\parallel})e^{in_1n_{\parallel}(\zeta-\eta)}F_{\mathrm{m}}\left[-n_3(\chi-\Lambda),n_{\parallel}\right]\times e^{in_2\sqrt{1-(n_3n_{\parallel}/n_2)^2}(\xi+\Lambda)}dn_{\parallel}, \tag{2.1.14}$$

Lastly, the scattered-transmitted field Ψ^1_{st}, transmitted through the interface at $\xi=0$ can be written as:

$$\Psi^1_{\mathrm{st}}(\xi,\zeta)=\psi_0\sum_{\mathrm{m}=-\infty}^{\infty}c_{\mathrm{m}}TW^1_{\mathrm{m}}(\xi,\zeta,\chi) \qquad \xi<0, \tag{2.1.15}$$

where

$$TW^1_{\mathrm{m}}(\xi,\zeta;\chi)=\frac{1}{2\pi}\int_{-\infty}^{\infty}T_{21}(n_{\parallel})T_{32}(n_{\parallel})e^{in_3n_{\parallel}(\zeta-\eta)}F_{\mathrm{m}}\left[-n_3(\chi-\Lambda,n_{\parallel})\right]e^{-i\sqrt{1-(n_3n_{\parallel})^2}\xi}dn_{\parallel}\,, \tag{2.1.16}$$

The equations for fields derived above, are presented using the Cartesian coordinates. Applying boundary conditions on the surface of the cylinder can be a lot easier

if the fields present in medium 3 are expressed in polar coordinates with respect to the reference frame centered at the scatterer, i.e., the SRF defined earlier. Therefore, Eqs. (2.1.5) and (2.1.9) are transformed from the cartesian to polar coordinates, respectively, as:

$$\Psi_{\mathrm{t3}}(\xi,\zeta) = \psi_0 T_{12}(n_{\parallel}) T_{23}(n_{\parallel}) e^{in_3\left[n_{\perp}^{t3}(\chi-\Lambda)+n_{\parallel}{}^{t3}\eta\right]} \sum_{\ell=-\infty}^{N} i^{\ell} J_{\ell}(n_3\rho) e^{i\ell\theta} e^{i\ell\theta_{t3}}\,, \tag{2.1.17}$$

and

$$\Psi_{sr}(\xi,\zeta) = \psi_0 \sum_{\ell=-\infty}^{\infty} J_{\ell}(n_3\rho) e^{i\ell\theta} \sum_{m=-\infty}^{\infty} c_{\mathrm{m}} RW_{m-\ell}\left[-n_3 2(\chi-\Lambda), n_3\eta\right]\,, \tag{2.1.18}$$

Using the boundary conditions on the surface of the cylinder for the TM and TE polarization, respectively, we have:

$$\mathrm{TM}: \quad \Psi_{\mathrm{t3}} + \Psi_{\mathrm{s}} + \Psi_{\mathrm{sr}}|_{\rho=k_o\alpha} = 0\,, \tag{2.1.19}$$

$$\mathrm{TE}: \quad \frac{\partial}{\partial\rho_{\mathrm{p}}}(\Psi_{\mathrm{t3}} + \Psi_{\mathrm{s}} + \Psi_{\mathrm{sr}})\Big|_{\rho=k_o\alpha} = 0\,, \tag{2.1.20}$$

Putting Eqs. (2.1.6), (2.1.17), and (2.1.18) in Eq. (2.1.20) and rearranging, we get:

$$\sum_{\mathrm{m}=-\infty}^{\infty} A_{\mathrm{m}\ell}^{(TM,TE)} c_{\mathrm{m}} = B_{\mathrm{m}}^{(TM,TE)}\,, \qquad \ell = 0; \pm1; \pm2..., \tag{2.1.21}$$

where

$$A_{\mathrm{m}\ell}^{(TM,TE)} = e^{-i\ell\theta_{t3}}[i^{-\ell} G_{\ell}^{(TM,TE)}(n_3\rho) RW_{\mathrm{m}-\ell}(-2n_3(\chi_{\mathrm{p}-\Lambda),\mathrm{n}_3\eta_{\mathrm{p}})} + \delta_{m\ell}]\,, \tag{2.1.22}$$

and

$$B_{\ell}^{(TM,TE)} = -G_{\ell}^{(TM,TE)}(n_3\rho) T_{12}(n_{\parallel}^{i}) T_{23}(n_{\parallel}^{i}) e^{in_3\left[n_{\perp}^{\mathrm{t3}}(\chi_{\mathrm{p}}-\Lambda)+n_{\parallel}^{\mathrm{t3}}\eta_{\mathrm{p}}\right]} e^{-i\ell\varphi_{\mathrm{t3}}}\,, \tag{2.1.23}$$

where $\delta_{m\ell}$ symbolizes the Kronecker delta and

$$\begin{aligned} G_{\ell}^{(\mathrm{TM})} &= \frac{J_{\ell}(x)}{H_{\ell}^{(1)}(x)}\,, \\ G_{\ell}^{(\mathrm{TE})} &= \frac{J_{\ell}'(x)}{H_{\ell}'^{(1)}(x)}\,. \end{aligned} \tag{2.1.24}$$

Once coefficient c_{m} is calculated after solving the linear system (2.1.21), we can calculate the required fields at any point (ξ, ζ) outside the cylinder. Moreover, we can also calculate the total scattered field.

Chapter 3

Numerical Implimentation

3.1 Validation of Code

For numerical implementation, the linear system is solved in eq. (2.1.21), by truncating the infinite order of the series expansions on cylindrical functions to $M = 3n_2a$ [71]. For the validation of the results, in Fig. 3.1 blue solid line is obtained and is cross-checked with the literature [71]. The self-consistency of code was further checked for an extra care. It was considered that the layered medium and the host medium has the same refractive index, i.e. $n_2 = n_3$ and we obtained the plot illustrated in red dotted line in Fig. 3.1. The result produced in Fig. 3.1 shows a perfect matched with the results reported in [**?**]. The developed algorithm turned out to be efficient and accurate and allows to calculate the results for the near and far fields.

3.2 Excitation without Cylinder

To study the scattering of SPP waves, we have chosen an interface of aluminum ($n_2 = \sqrt{-54 + 21i}$) and air ($n_3 = 1$) for the propagation of these waves. Furthermore, the TKR prism-coupled configuration is chosen to excite SPP waves using a dense prism of refractive index ($n_1 = 2.6$). The operating wavelength is chosen as 633 nm.

To find the angle θ_{spp}, the SPP wave can be excited, the reflectance and transmittance were computed as a function of the incidence angle ϕ_i are presented in Fig. 3.2. The reflectance dip at $\phi_i = \theta_{\text{SPP}} = 22.9^o$ indicates the excitation of the SPP

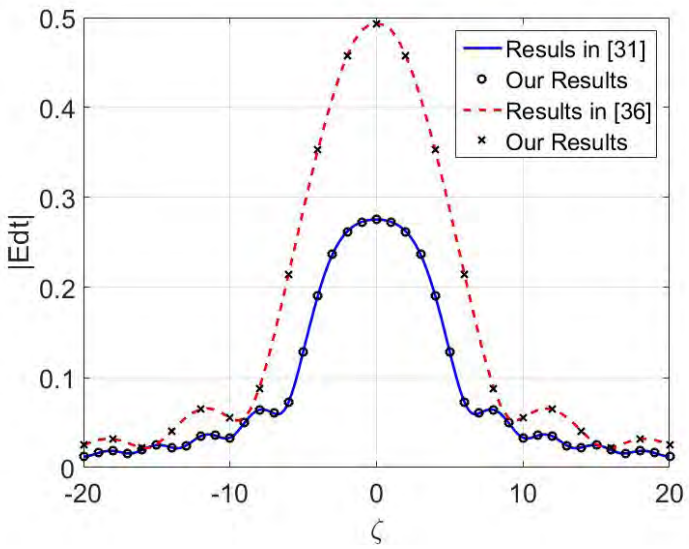

Figure 3.1: Magnitude of scattered transmitted field |Edt| plotted in blue solid line from buried cylinder below a dielectric slab, at $\xi = -0.1$, when $\alpha = 1, \chi = 5, \Lambda = 1, \epsilon_{r1} = 2.25, \epsilon_{r2} = 9$, TM polarization. Magnitude of scattered transmitted field |Edt| plotted in red dotted line from buried cylinder in a dielectric half space, when $\phi_i = 0$, $\alpha = 1$, $n_1 = 1$ $n_2 = n_3 = 2$ and $\chi = \alpha + \pi/2$, TM polarization.

wave. This is further confirmed by the variation of the magnitude of the magnetic field around the metal/air interface in Fig. 3.3 since the field is strong at the interface and decays away from the interface.

3.3 Backward-Scattered Near-field

To see the effect of SPP waves on the scattering, the backward-scattered fields in medium 1 are computed at $x = -0.5$ nm when the incidence angle is the same that excites the SPP waves and when the incidence angle is different, as shown in Fig. 3.4 and 3.5, respectively. Both the effect of the size of the cylinder and the distance from the metal/medium3 interface is analyzed. Since SPP wave is localized to the interface, an object nearer the interface should scatter more than the one further away from the interface. From both of these figures, it can be clearly seen that the scattering of light is much more pronounced when the SPP wave is excited than when

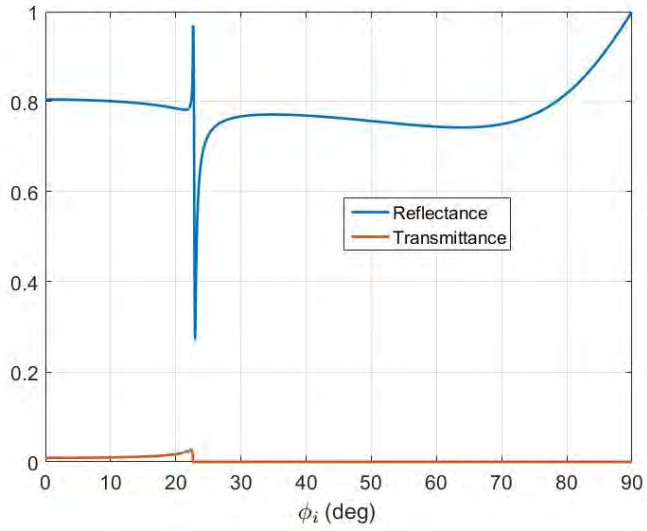

Figure 3.2: The reflectance and transmittance of the layered structure in the absence of circular cylinder as a function of the incidence angle of the incident plane waves when $n_1 = 2.6$, $n_2 = \sqrt{-54 + 21i}$ and $n_3 = 1$ and $L = 15$ nm. The excitation of SPP wave is indicated by the reflectance dip at $\theta_{\text{spp}} = 22.9^o$

it is not. The results for $\phi_i = 12.9^0$ for the case of SPP wave not being excited are shown and the similar behavior is noted as long as ϕ_i is away from the reflectance dip, either greater or smaller than θ_{SPP}.

A further analysis of Figs. 3.4 and 3.5 shows that the scattered field is about 10 times stronger when the SP waves is present for similar values of a and h than when the SPP wave is not present. Therefore, the scattering is definitely affected by the presence of SPP waves. Also, the scattered field becomes smaller when either the size of the scatter is decreased or it is moved away from the interface.

3.4 Forward-Scattered Near-field

To understand the effect of the presence of the cylindrical scatter near an SPP wave, the total field around it is examined and compared with the case when the SPP wave is not excited. For this purpose, the magnitude of magnetic field of the total scattered field $|H_{ts}| = |\Psi_s + \Psi_{sr}|$ in medium 1, $|\Psi^2_{st} + \Psi^2_{sr}|$ in medium 2 and in $|\Psi^1_{st}|$ is plotted

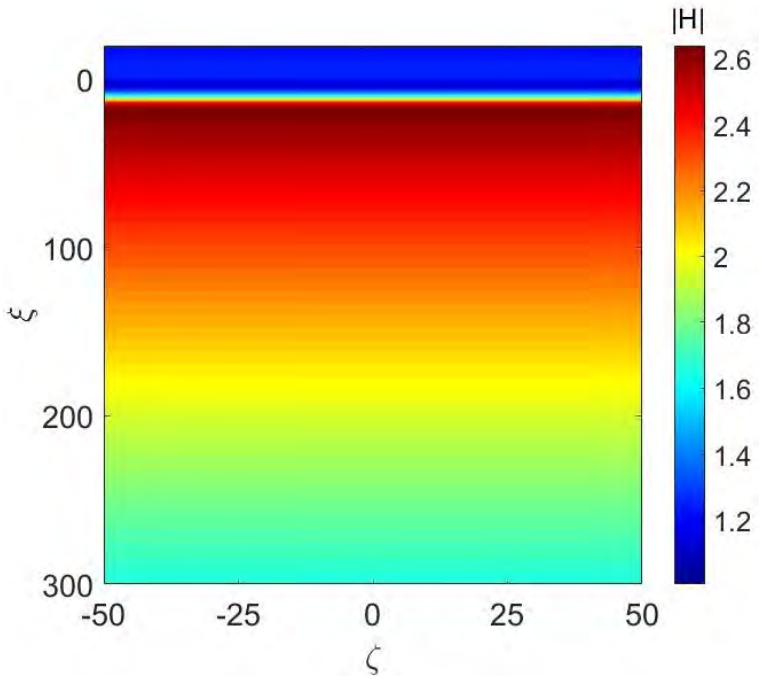

Figure 3.3: Variation of magnitude of SPP wave at $\phi_i = \theta_{\text{spp}} = 22.9$ deg in the absence of circular cylinder, when $n_1 = 2.6$, $n_2 = \sqrt{-54 + 21i}$, $n_3 = 1$, and $L = 15$ nm.

as a function of ξ and ζ in Figs. 3.6 and 3.7. A simple comparison of both figures indicate that the fields around the cylinder are much stronger when the SPP wave is present than when it is not. Furthermore, not surprisingly, the dipole mode is being excited in the cylinder. However, one major difference is that the axis of this dipole is parallel to the interface when the SPP wave is present, whereas, the axis is function of the incidence angle when the SPP wave is not present.

3.5 Backward-scattered Far-Field

For better understanding of the effect of SPP waves on the scattered field, the far-fields in medium 1 are computed when incident angles are $\phi_i = \theta_{\text{SPP}} = 22.9^o$ and $\phi_i = 12.9^o$ as shown in Figs. 3.8 and 3.9, respectively, as a function of the angle of field propagation with the positive ξ axis. Both the effect of the size of the cylinder

and the distance from the metal/medium3 interface is analyzed. A comparison of both figures shows that the backward-scattered field is almost twice in strength when the SPP wave is excited than when when the SPP wave is not excited for the same values of a and h. Moreover, the scattering in both cases has a peak around $\theta_s = 180^o - \phi_i$ in rough accordance with the Snell's law due to the presence of the cylinder since the incidence is at $\theta_s = 180^o + \phi$.

3.6 Forward-scattered Far-Field

Now, the far zone scattered field in medium 3 was computed to see the effect of scattering of the SPP waves. As the expansion coefficients c_m are known, the asymptotic method leads to the evaluation of the far-field by means of relation (38) of [**?**]. The far-field scattered in the forward direction is shown in Figs. 3.10 and 3.11, respectively, for $\phi = \theta_{\text{SPP}} = 22.9^o$ and $\phi = 12.9^o$, when the reflecting surface is the interface between metallic layer and medium 3, for various values of a and h. A comparison of these two figures shows that the forward far zone scattered field is much stronger for incidence angle θ_{SPP}. Also, the increase in radius of cylinder has more significant effect than increase in depth at the scattered field. This could be due to the increase in the energy of the excitations of cylinder due to increase in scattering surface when radius of the cylinder is increased.

In Figs. 3.10 and 3.11, the forward scattering is maximum in the region $\theta_s \in (-90^o, 0^o)$. This is because the incident light excites the cylinder and makes it like a dipole with more strength on the left side (see Figs. 3.6 and 3.7). The higher strength on the left side of dipole results in higher strength of the scattered field on this side. A comparison of both figures shows that the forward scattering can be as high as several times when the SPP wave is excited than when it is not.

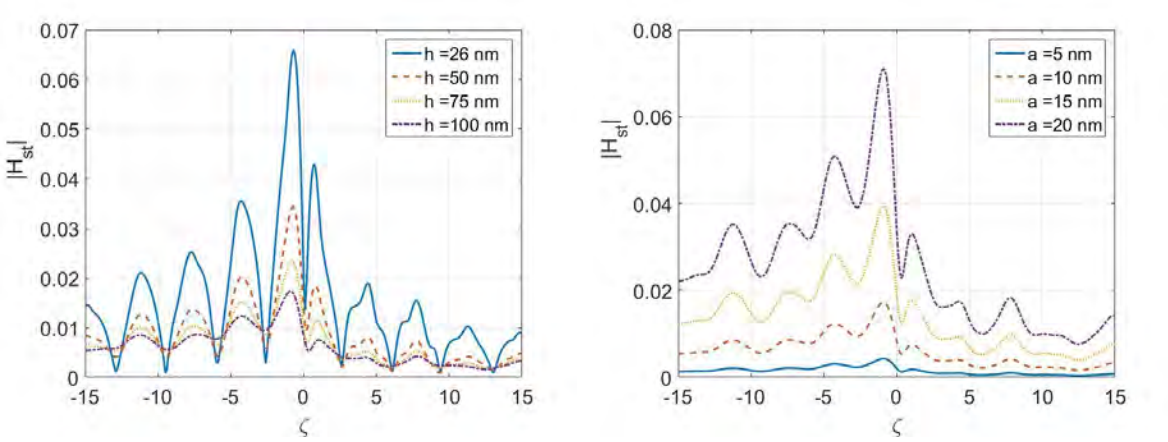

(a) a=10 nm (b) h=100 nm

Figure 3.4: Near zone scattered-transmitted field in medium 1 when $\phi_i = \theta_{\text{spp}} = 22.9^0$.

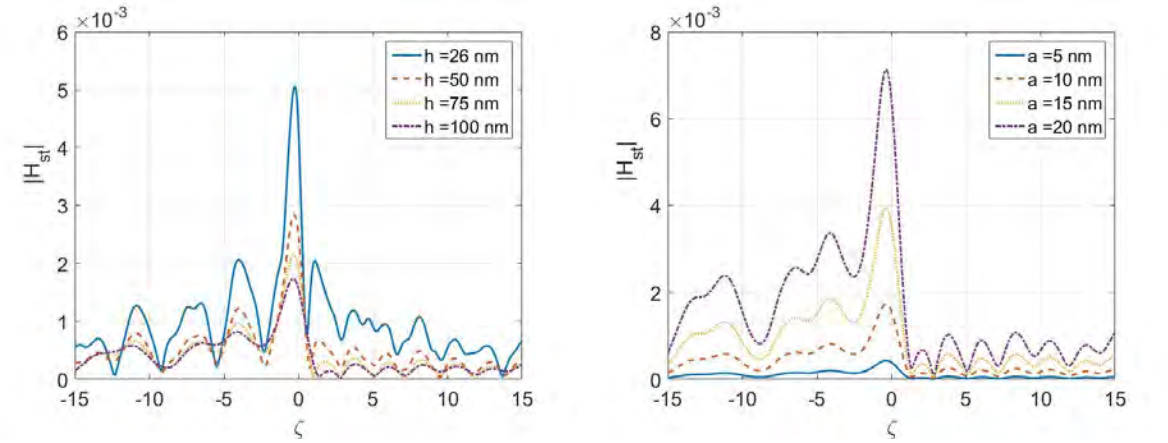

(a) a=10 nm (b) h=100 nm

Figure 3.5: Near zone scattered-transmitted field in medium 1 $\phi_i = 12.9^0$.

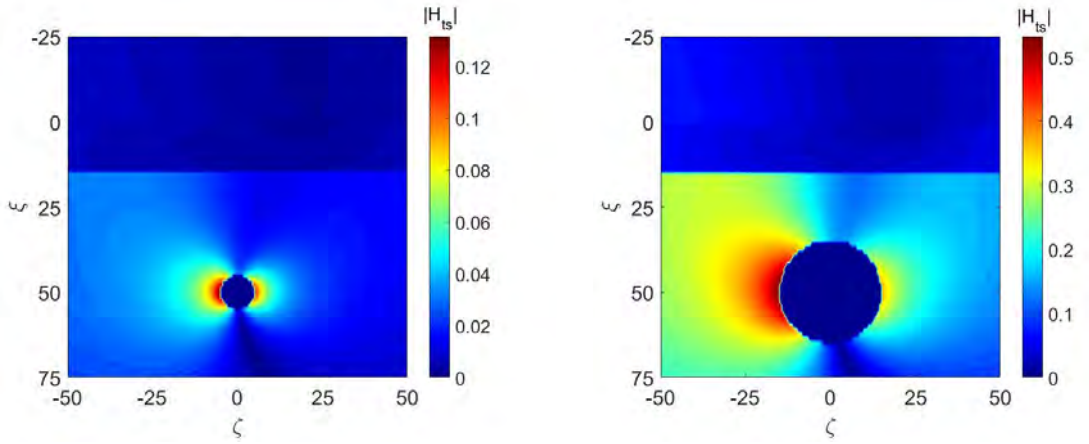

(a) $a = 5$ nm, $h = 50$ nm (b) $a = 15$ nm, $h = 50$ nm

Figure 3.6: Total scattered fields when $\phi_i = \theta_{\text{spp}} = 22.9^o$

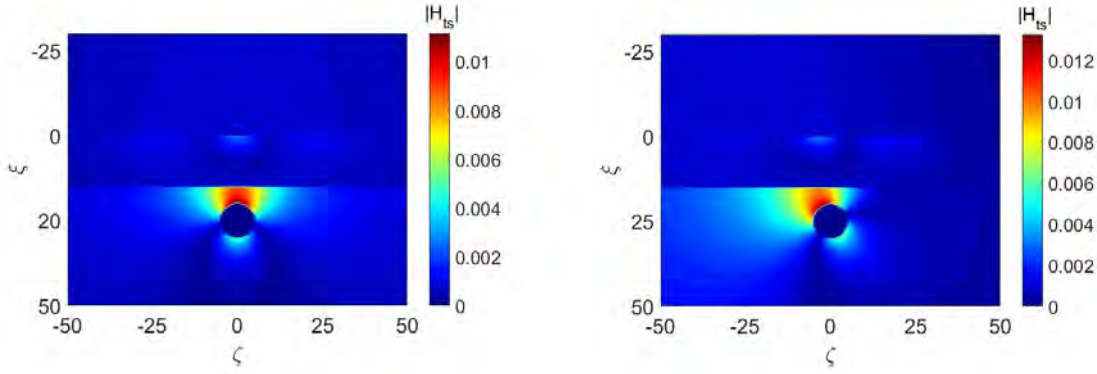

(a) $\phi_i = 0^o$ (b) $\phi_i = 12.9^o$

Figure 3.7: Total scattered field when $a = 5$ nm, and $h = 25$ nm.

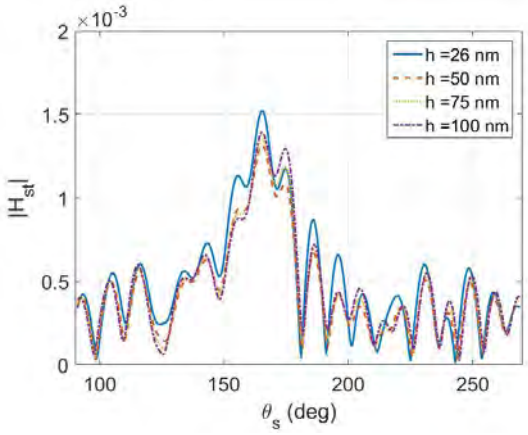

(a) a=10 nm

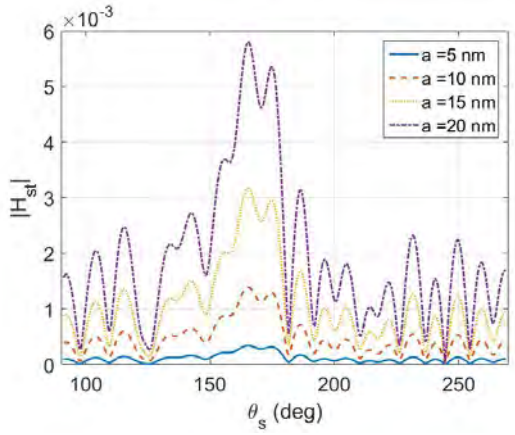

(b) h=100 nm

Figure 3.8: Backward-scattered far-field field in medium 1 $\phi_i = \theta_{\text{SPP}} = 22.9$. The angle θ_s is measured with the positive ξ axis.

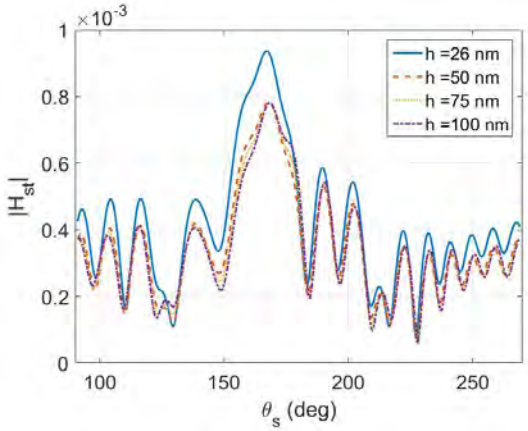

(a) a=10 nm

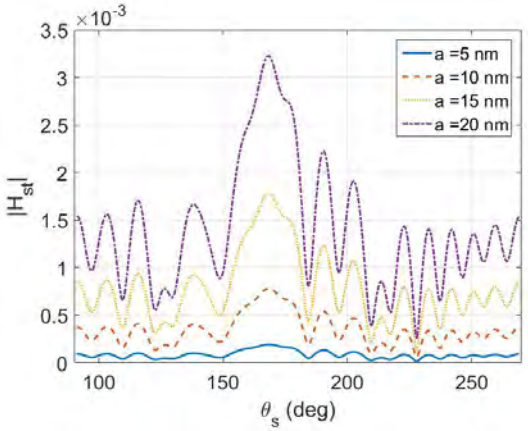

(b) h=100 nm

Figure 3.9: Backward-scattered far-field in medium 1 $\phi_i = 12.9$. The angle θ_s is measured with the positive ξ axis.

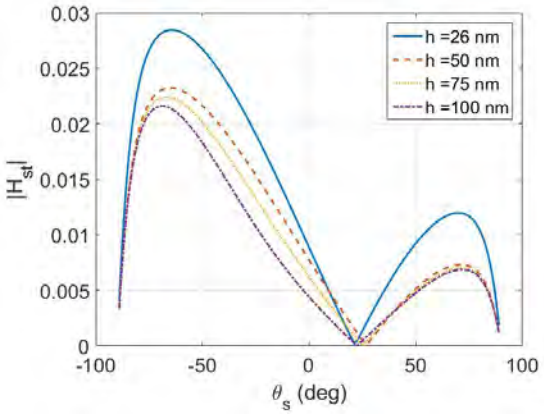

(a) a=10 nm

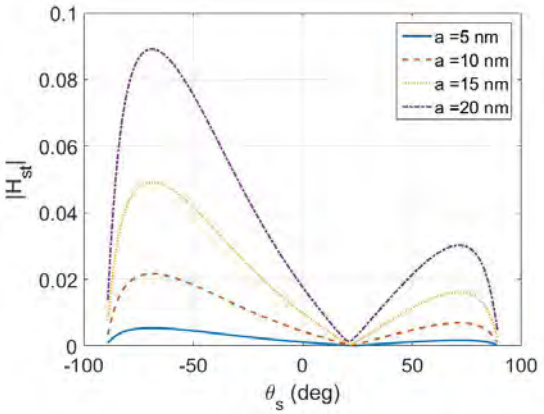

(b) h=100 nm

Figure 3.10: Forward-scattered far-field in medium 3 when $\phi_i = \theta_{\text{SPP}} = 22.9$.

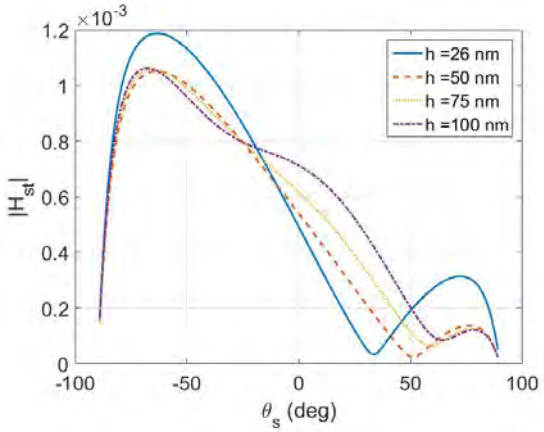

(a) a=10 nm

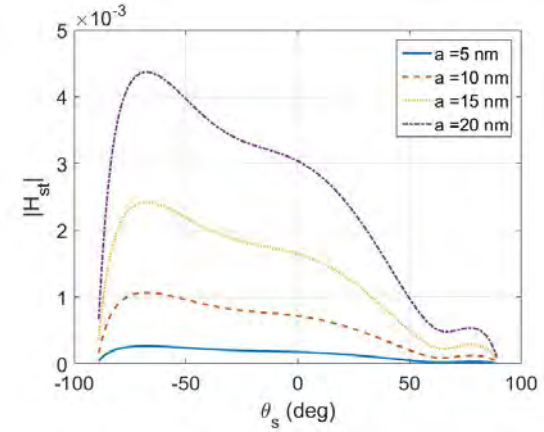

(b) h=100 nm

Figure 3.11: Forward-scattered far-field in medium 3 when $\phi_i = 12.9$.

Conclusion

The scattering of surface plasmon-polariton (SPP) waves by a PEC circular cylinder was delineated. The problems was formulated using the cylindrical wave approch and both the near and far fields were investigated by considering the PEC cylinder close or away from the SPP-wave-guiding interface of a metallic strip and an isotropic dielectric material. The SPP wave was excited in a practical prism-coupled configuration. The investigations showed that the presence of the circular cylinder near the metallic interface increases the scattering, but the scattering is significantly higher when the SPP wave is excited and can be as high as several times. Furthermore, the forward scattering is higher in the region $\theta_s \in (90^o, 180^o)$ and the backward scattering is higher for $\theta_s \in (-90^o, 0^o)$.

References

[1] Barnes, William L and Dereux, Alain and Ebbesen, Thomas W, *Surface plasmon subwavelength optics*, nature, volume 424 number 6950, pages 824-830, Nature Publishing Group (2003)

[2] Zayats, Anatoly V and Smolyaninov, Igor I, *Near-field photonics: surface plasmon polaritons and localized surface plasmons*, Journal of Optics A: Pure and Applied Optics, volume 5, pages S16, IOP Publishing (2003)

[3] Sekhon, Jagmeet Singh and Verma, SS, *Plasmonics: the future wave of communication*, Current Science, volume 101, pp. 484-488, JSTOR (2011)

[4] Leuthold, Juerg and Hoessbacher, C and Muehlbrandt, S and Melikyan, A and Kohl, M and Koos, C and Freude, W and Dolores-Calzadilla, V and Smit, M and Suarez, I and others, *Plasmonic communications: light on a wire*, Optics and Photonics News, volume 24, pp. 28-35, Optical Society of America (2013)

[5] Maier, Stefan Alexander, Plasmonics: fundamentals and applications, Springer Science & Business Media (2007)

[6] Agrahari, Rajan and Lakhtakia, Akhlesh and Jain, Pradip K, *Information carried by a surface-plasmon-polariton wave across a gap*, Journal of Applied Physics, volume 124, pp. 053104, AIP Publishing LLC (2018)

[7] Zhang, Hao Chi and Liu, Shuo and Shen, Xiaopeng and Chen, Lin Hui and Li, Lianming and Cui, Tie Jun, *Broadband amplification of spoof surface plasmon polaritons at microwave frequencies*,

[8] C. J. Bouwkamp, *On Sommerfeld's surface wave*, Phys. Rev. 80, 294-294 (1950).

[9] H. M. Barlow, *Radio Surface Waves*, Clarendon Press (1962).

[10] A. D. Boardman (Ed.), *Electromagnetic Surface Modes*, Wiley, Chicester, United Kingdom (1982).

[11] J. Zenneck, *Uber die Fortpflanzung ebener elektromagnetischer Wellen langs einer ebenen Lieterfl ache und ihre Beziehung zur drahtlosen Telegraphie*, Ann. Phys. Lpz. 23, 846-866 (1907).

[12] A. Sommerfeld, *Uber die Ausbreitung der Wellen in der drahtlosen Tele-graphie*, Ann. Phys. Lpz. 28, 665-736 (1909).

[13] D. A. Hill and J. R. Wait, *On the excitation of the Zenneck surface wave over the ground at 10 MHz*, Ann. Telecommun. 35, 179-182 (1980).

[14] V. N. Datsko and A. A. Kopylov, *On surface electromagnetic waves*, Sov. Phys. Usp. 51, 101-102 (2008).

[15] R. H. Ritchie and H. B. Eldridge, *Optical emission from irradiated foils. I*, Phys. Rev. 126, 1935-1947 (1962).

[16] S. A. Maier, *Plasmonics: Fundamentals and Applications*, Springer, New York, USA (2007).

[17] M. Dragoman and D. Dragoman, *Plasmonics: Applications to nanoscale terahertz and optical devices*, Prog. Quantum Electron. 32, 1-41 (2008).

[18] M. G. Blaber, M. D. Arnold, and M. J. Ford, *A review of the optical properties of alloys and intermetallics for plasmonics*,J. Phys.: Condens. Matter 22, 143201 (2001).

[19] J. A. Polo Jr. and A. Lakhtakia, *Surface electromagnetic waves: A review*, Laser Photon. Rev. 5, 234-246 (2011).

[20] P. R. West, S. Ishii, G. V. Naik, N. K. Emani, V. M. Shalaev, and A. Boltasseva, *Searching for better plasmonic materials*, Laser Photon. Rev. 4, 795-808 (2010).

[21] G. Borstel and H. J. Falge, *Surface phonon-polaritons*, in Ref. 7.

[22] R. F. Wallis, *Surface magnetoplasmons on semiconductors*, in Ref. 7.

[23] S. J. Elston and J. R. Sambles, *Surface plasmon-polaritons on an anisotropic substrate*,J. Mod. Opt. 37, 1895-1902 (1990).

[24] R. A. Depine and M. L. Gigli, *Excitation of surface plasmons and total absorption of light at the flat boundary between a metal and a uniaxial crystal*, Opt. Lett. 20, 2243-2245 (1995).

[25] H. Wang, *Excitation of surface plasmon oscillations at an interface between anisotropic dielectric and metallic media*,Opt. Mater. 4, 651-656 (1995).

[26] R. A. Depine and M. L. Gigli, *Resonant excitation of surface modes at a single flat uniaxial-metal interface*, J. Opt. Soc. Am. A 14, 510-519 (1997).

[27] W. Yan, L. Shen, L. Ran, and J. A. Kong, *Surface modes at the interfaces between isotropic media and indefinite media*, J. Opt. Soc. Am. A 24, 530-535 (2007).

[28] I. Abdulhalim, *Surface plasmon TE and TM waves at the anisotropic filmmetal interface*, J. Opt. A: Pure Appl. Opt. 11, 015002 (2009).

[29] J. A. Polo Jr. and A. Lakhtakia, *On the surface plasmon polariton wave at the planar interface of a metal and a chiral sculptured thin film*, Proc. R. Soc. Lond. A 465, 87-107 (2009).

[30] J. A. Polo Jr. and A. Lakhtakia, *Energy flux in a surface-plasmon-polariton wave bound to the planar interface of a metal and a structurally chiral material*, J. Opt. Soc. Am. A 26, 1696-1703 (2009).

[31] G. J. Sprokel, R. Santo, and J. D. Swalen, *Determination of the surface tilt angle by attenuated total reflection*, Mol. Cryst. Liq. Cryst. 68, 29-38 (1981).

[32] G. J. Sprokel, *The reflectivity of a liquid crystal cell in a surface Plasmon experiment*, Mol. Cryst. Liq. Cryst. 68, 39-45 (1981).

[33] R. Haupt and L. Wendler, *Dispersion and damping properties of Plasmon polaritons in superlattice structures II. Semi-infinte superlattice*, Phys. Status Solidi B 142, 423-435 (1987).

[34] J. A. Gaspar-Armenta and F. Villa, *Photonic surface-wave excitation: photonic crystal-metal interface*, J. Opt. Soc. Am. B 20, 2349-2354 (2003).

[35] R. Das and R. Jha, *On the modal characteristics of surface plasmon polaritons at a metal-Bragg interface at optical frequencies*, Appl. Opt. 48, 4904-4908 (2009).

[36] Y.-J. Jen, A. Lakhtakia, C.-W. Yu, and T.-Y. Chan, *Multilayered structures for p- and s-polarized long-range surface-plasmon-polariton propagation*, J. Opt. Soc. Am. 26, 2600-2606 (2009).

[37] J. Homola (Ed.), Surface Plasmon Resonance Based Sensors, Springer, Heidelberg, Germany (2006).

[38] I. Abdulhalim, M. Zourob, and A. Lakhtakia, *Surface plasmon resonance for biosensing: A mini-review*, Electromagnetics 28, 214-242 (2008).

[39] I. Abdulhalim, M. Zourob, and A. Lakhtakia, *Handbook of Biosensors and Biochips Eds.*, R Marks, D Cullen, I Karube, C R Lowe, and H H Weetall, Wiley, Chichester 413-46 (2007).

[40] K. U.-Aoki, K. Shimada, M. Nagano, M. Kawai, and H. Koga, *A novel approach to protein expression profiling using antibody microarrays combined with surface plasmon resonance technology*,Proteomics 5, 2396-2401 (2005).

[41] V. Kanda, P. Kitov, D. R. Budle, and M. T. McDermott, *Surface Plasmon resonance imaging measurements of the inhibition of Shiga-like toxin by synthetic multivalent inhibitors*, Anal. Chem. 77, 7497-7504 (2005).

[42] P. G. Kik, S. A. Maier, and H. A. Atwater, *Plasmon printing-A new approach to near-field lithography*,MRS Symp. Proc. 705, Y3.6 (2002).

[43] S. A. Maier, M. L. Brongersma, P. G. Kik, S. Meltzer, A. A. G. Requicha, and H. A. Atwater, *Plasmonics-A route to nanoscale optical devices*, Adv. Mater. 13, 1501-1505 (2001).

[44] P. Berini, *Long-range surface plasmon polaritons*, Adv. Opt. Photon. 1, 484-588 (2009).

[45] T. G. Mackay and A. Lakhtakia, *Modeling columnar thin films as platforms for surface-plasmonic-polaritonic optical sensing*, Photon. Nanostruct. Fund. Appl. 8, 140-149 (2010).

[46] Devender, D. P. Pulsifer, and A. Lakhtakia, *Multiple surface plasmon polariton waves*, Electron. Lett. 45, 1137-1138 (2009).

[47] A. Lakhtakia, Y.-J. Jen, and C.-F. Lin, *Multiple trains of same-color surface plasmon-polaritons guided by the planar interface of a metal and a sculptured nematic thin film. Part III: Experimental evidence*, J. Nanophoton. 3, 033506 (2009).

[48] J. A. Gaspar-Armenta and F. Villa, *Photonic surface-wave excitation: photonic crystal-metal interface*, J. Opt. Soc. Am. B 20, 2349-2354 (2003).

[49] W. M. Robertson and M. S. May, *Surface electromagnetic wave excitation on one-dimensional photonic band-gap arrays*, Appl. Phys. Lett. 74, 1800-1802 (1999).

[50] Z. Salamon, H. A. Macleod, and G. Tollin, *Coupled plasmon-waveguide resonators: A new spectroscopic tool for probing proteolipid film structure and properties*, Biophys. J. 73, 2791-2797 (1997).

[51] Z. Salamon and G. Tollin, *Optical anisotropy in lipid bilayer membrane: Coupled plasmon-waveguide resonance measurements of molecular orientation, polarizability, and shape*, iophys. J. 80, 1557-1567 (2001).

[52] J. Moreland, A. Adams, and P. K. Hansma, *Efficiency of light emission from surface plasmons*,em Phys. Rev. B 25, 2297-2300 (1982).

[53] P. T. Worthing and W. L. Barnes, *Efficient coupling of surface plasmon polaritons to radiation using a bi-grating*, Appl. Phys. Lett. 79, 3035-3037 (2001).

[54] W. L. Barnes, A. Dereux, and T. W. Ebbesen, *Surface plasmon subwavelength optics*, Nature 424, 824-830 (2003).

[55] P. V. Lambeck, *Integrated optical sensors for the chemical domain*, Meas. Sci. Technol. 17, R93-R116 (2006).

[56] Howard, A. Q., *The electromagnetic fields of a subterranean cylindrical inhomogeneity excited by a line source*, Geophys., Vol. 37, 975-984, Dec. 1972.

[57] Lambert, M., *The scattering by a cylindrical dielectric obstacle buried in a half-space: a H-field-based solution method*, J. of Electromagnetic Waves and Appl., Vol. 9, 1129-1262, Sept. 1998.

[58] Parry, J. R. and S. H. Ward, *Electromagnetic scattering from cylinders of arbitrary cross-section in a conductive half-space*, Geophys., Vol. 36, 67-100, Feb. 1971.

[59] Moaveni, M. K., A. A. Rizvi, and B. A. Kamran, *Planewave scattering by gratings of conducting cylinders in an inhomogeneous and lossy dielectric*, J. Opt. Soc. Am. A, Vol. 5, 834-842, 1988.

[60] Ogunade, S. O., *Electromagnetic response of an embedded cylinder for line current excitation*, Geophys., Vol. 46, 45-52, Jan. 1981.

[61] D'Yakonov, B. P., *The diffraction of electromagnetic waves by a circular cylinder in a homogeneous half-space*, Bull. Acad. Sci. U.S.S.R., Geophysics, ser. No. 9, 950-955, 1959.

[62] Mahmoud, S. F., S. M. Ali, and J. R. Wait, *Electromagnetic scattering from a buried cylindrical inhomogeneity inside a lossy earth*, Radio Sci., Vol. 16, No. 6, 1285-1298, 1981.

[63] Butler, C. M., X. B. Xu, and A. W. Glisson, *Current induced on a conducting cylinder located near the planar interface between two semi-infinite half-spaces*, IEEE Trans. Antennas Propagat., Vol. AP-33, 616-624, June 1985.

[64] Hongo, K. and A. Hamamura, *Asymptotic solutions for the scattered field of plane wave by a cylindrical obstacle buried in a A spectral-domain solution for the scattering problem 251 dielectric half-space*, IEEE Trans. Antennas Propagat., Vol. AP- 34, 1306-1312, Nov. 1986.

[65] Sneddon, I. N., *Mixed Boundary Value Problems in Potential Theory*, North-Holland, Amsterdam, 1966.

[66] Naqvi, Q. A., A. A. Rizvi, and Z. Yaqoob, Corrections to: *Asymptotic solutions for the scattered fields of plane wave by a cylindrical obstacle buried in a dielectric half-space*, IEEE Trans. Antennas Propagat., Vol. AP-48, 846-848, May 2000.

[67] K. A. Michalski and D. Zheng, *Electromagnetic scattering and radiation by surfaces of arbitrary shape in layered media, part I: Theory*, IEEE Trans. Antennas Propag., vol. 38, no. 3, Mar. 1990.

[68] P. C. Chang, R. J. Burkholder, J. L. Volakis, R. J. Marhefka, and Y. Bayram, *High-frequency EM characterization of through-wall building imaging*, IEEE Trans. Geosci. Remote Sens., vol. 47, no. 5, pp. 1375-1387, 2009.

[69] F. Frezza, L. Pajewski, C. Ponti, and G. Schettini, *Through-wall electromagnetic scattering by N conducting cylinders*, J. Opt. Soc. Amer. A, vol. 30, no. 8, pp. 1632-1639, Aug. 2013.

[70] M. A. Fiaz, C. Ponti, and G. Schettini, *On the scattering by a cylindrical object below a rough surface with the CWA*, presented at the IEEE MTT-S Int. Conf.

Numer. Electromagn. Model. Optim. RF, Microw., THz Appl., Pavia, Italy, May 14-16, 2014.

[71] C. Ponti and S. Vellucci, *Scattering by Conducting Cylinders Below a Dielectric Layer With a Fast Noniterative Approach*, in IEEE Transactions on Microwave Theory and Techniques, vol. 63, no. 1, pp. 30-39, Jan. 2015.

[72] F. Ciambra, F. Frezza, L. Pajewski and G. Schettini (2003) *A spectral-domain solution for the scattering problem of a circular cylinder buried in a dielectric half-space*, Abstract, Journal of Electromagnetic Waves and Applications, 17:4, 607-609

[73] T. Turbadar, *Complete absorption of light by thin metal films*, Proceedings of the Physical Society , vol. 73, no. 1, p. 40, 1959

[74] E. Kretschmann and H. Raether, *Radiative decay of non radiative surface plasmons excited by light*, Zeitschrift fur Naturforschung A, vol. 23, no. 12, pp. 2135-2136, 1968.

[75] A. Otto, *Excitation of nonradiative surface plasma waves in silver by the method of frustrated total reflection*, Zeitschrift fur Physik A Hadrons and nuclei , vol. 216, no. 4, pp. 398-410, 1968